JHEP

Published for SISSA by Springer

Received: January 18, 2019
Revised: July 27, 2019
Accepted: August 29, 2019
Published: October 3, 2019

# Six top messages of new physics at the LHC

**Huayong Han,**[a] **Li Huang,**[b,c,d] **Teng Ma,**[b,d] **Jing Shu,**[b,c,e,f] **Tim M.P. Tait**[g] **and Yongcheng Wu**[h]

[a] *Guizhou Key Laboratory in Physics and Related Areas, Guizhou University of Finance and Economics, Guiyang 550025, China*
[b] *CAS Key Laboratory of Theoretical Physics, Institute of Theoretical Physics, Chinese Academy of Sciences, Beijing 100190, China*
[c] *School of Physical Sciences, University of Chinese Academy of Sciences, Beijing 100049, China*
[d] *Laboratory for Elementary Particle Physics, Cornell University, Ithaca, NY 14853, U.S.A.*
[e] *CAS Center for Excellence in Particle Physics, Beijing 100049, China*
[f] *Center for High Energy Physics, Peking University, Beijing 100871, China*
[g] *Department of Physics and Astronomy, University of California, Irvine, CA 92697, U.S.A.*
[h] *Ottawa-Carleton Institute for Physics, Carleton University, 1125 Colonel By Drive, Ottawa, Ontario K1S 5B6, Canada*

*E-mail:* hhycqu@mail.gufe.edu.cn, huangli@ku.edu, t.ma@campus.technion.ac.il, jshu@itp.ac.cn, ttait@uci.edu, ycwu@physics.carleton.ca

Abstract: Six top signatures provide a novel probe of new physics. We discuss production of six top quarks as the decay products of a pair of top partners in the setting of a composite Higgs model, and argue that the six top signal may generically provide one of the first final states to show a discrepancy. We construct an analysis based on quantities such as $H_T$ and the numbers of jets which are tagged as boosted tops, $W$s, or containing $b$-tags, and show that the LHC with 3 ab$^{-1}$ can discover top partners with masses up to around 2.5 TeV in the six top signature.

Keywords: Beyond Standard Model, Technicolor and Composite Models

ArXiv ePrint: 1812.11286



https://doi.org/10.1007/JHEP10(2019)008

JHEP10(2019)008

## Contents



## 1 Introduction

The Large Hadron Collider (LHC), with its unparalleled energy and high luminosity, will definitively explore the physics at the TeV scale. The discovery of Higgs boson at the LHC is a triumph of the Standard Model (SM), however, the Naturalness problem associated with the self-energy of the Higgs particle argues that it is likely that there is new physics around the TeV scale [1–7]. Various new physics models addressing this problem have been proposed, such as Supersymmetry (SUSY), little Higgs, Composite Higgs etc. Deep investigation of the naturalness problem may reveal new details underlying the physics of the electroweak symmetry breaking (EWSB) and could also provide the evidence of new physics.

Beside the Higgs, the top quark is central to arguments concerning naturalness, since it has the largest mass of the SM fermions, and hence the largest coupling to the Higgs. For this reason, partners of the top quark are ubiquitous in models of new physics at the weak scale, and their production often results in multi-top signatures at the LHC, leading to many interesting phenomena.[1] The four top final state has been previously investigated [19–24] and is starting to be visible in experimental analysis [25, 26]. However, even more tops in the final state naturally occur if extral pseudo-Nambu-Goldstone bosons (pNGB) is introduced by extending the global symmetry of composite Higgs models [16] and provides a spectacular collider signature and a complementary method to search for new physics.

[1] Other studies searching for top-partners can be found in [8–18]



JHEP10(2019)008

In this paper, we systematically investigate the phenomenology of six-top final states in a simplified model inspired by a composite Higgs scenario. We estimate the sensitivity of the LHC to six-top final states for channels with different number of charged leptons, and the upper limit on the top partner branch ratio into $t\bar{t}t$ are obtained in the case that no signal is observed with 3 $\text{ab}^{-1}$ of integrated luminosity. We also discuss the extraction of the top partner mass. It should be stressed that six-top final states occur in many other models of new physics, and our general analysis framework can be applied to those cases with simple adjustments.

The paper is organized as follows. In section 2, we introduce a simplified composite Higgs model which inspires our analysis and in section 3 discuss general features of the six top signature and current LHC constraints. The analysis strategy of LHC data are described in section 4. We reserve section 5 for our conclusions.

## 2 Six tops from a general composite Higgs model

Generally, composite Higgs models with a simple UV completion (such as SU(4)/Sp(4) [27–29] or the isomorphic coset space SO(6)/SO(5) [30–32] and SU(4) × SU(4)/SU(4) [33–35]), contain a singlet scalar pseudo-Nambu-Goldstone boson (pNGB) field $s$ corresponding to a broken $\text{U}(1)_s$ global symmetry. This pNGB can decay into di-bosons through Wess-Zumino-Witten (WZW) terms via fermion loops. In theories with partial compositeness, $s$ can also decay into fermion pairs through the elementary-composite mixing terms between the SM fermions and the composite top partners $t'$. Since the decay into dibosons are effectively at loop level, and the large top mass implies in such theories that the top partners predominantly mix with the SM top, $s$ generically decays into a top pair with very close to 100% branch ratio (BR). Since $\text{U}(1)_s$ is always preserved in gauge sector and its breaking pattern in fermion sector depends on the embeddings of SM fermions to global symmetry, which can make $s$ mass lies in range from zero to the global symmetry breaking scale $f$. While the masses of composite top partners are normally at confine scale $\Lambda \sim 4\pi f$ so top partners are heavier than $s$ generically. The same large mixing generically implies that, provided the mass of the $s$ is not too large, the top partners themselves decay into $s$ and top with a significant BR. As a result, a single top partner typically undergoes the decay chain,

$$t' \to ts \to t\bar{t}t, \tag{2.1}$$

and an event originating from pair production of the top partners results in a six top final state (see figure 1 left panel):

$$p\ p \to \bar{t}'\ t' \to \bar{t}\ s\ t\ s \to \bar{t}\ t\ \bar{t}\ t\ \bar{t}\ t. \tag{2.2}$$

We work with an effective Lagrangian capturing the essential features of the interactions between top partners and $s$. Requiring that the singlet $s$ renormalizably couples to the top and its partner, the vector-like top partners must either be electroweak singlets ($T = t'$) or doublets ($\psi = (t', b')$) with hypercharge $Y = 1/6$. In the first (singlet) case, the effective Lagrangian reads

$$\mathscr{L} = \bar{T}(i\not{D} - m_{t'})T + \frac{1}{2}\partial_\mu s \partial^\mu s - \frac{1}{2}m_s^2 s^2 - \lambda\ s\bar{T}_L t_R - \lambda_1 \bar{q}_L H T_R - \lambda_2 f \bar{T}_L t_R + \text{h.c.} \tag{2.3}$$



JHEP10(2019)008

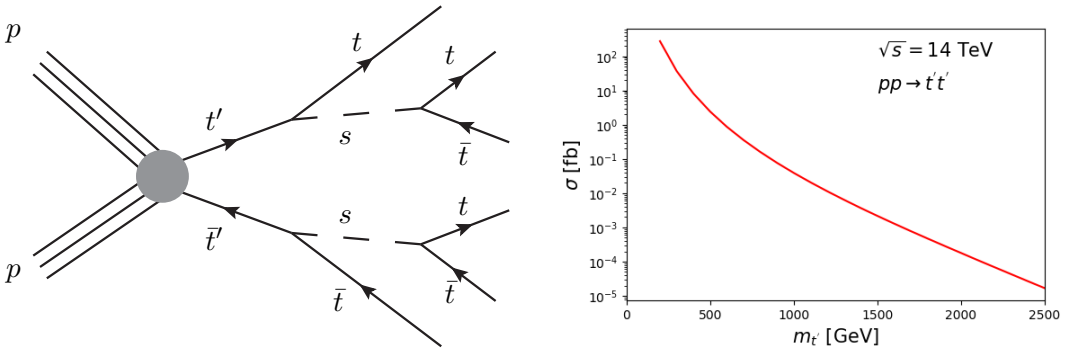


**Figure 1**. Left: representative Feynman diagram for a 6 top final state through top-partner pair production. Right: the cross section for top-partner pair production at the LHC with $\sqrt{s} = 14\,\text{TeV}$ as function of top-partner mass.

And the doublet case is described by

$$\mathscr{L} = \bar{\psi}(i\not{D} - m_{t'})\psi + \frac{1}{2}\partial_\mu s \partial^\mu s - \frac{1}{2}m_s^2 s^2 - \lambda\ s\bar{\psi}_R q_L - \lambda_1 \bar{\psi}_L H t_R - \lambda_2 f \bar{\psi}_R q_L + \text{h.c.} \quad (2.4)$$

Here $H$ is the SM Higgs doublet field, $D_\mu$ is the appropriate covariant derivative, $m_{t'}$ and $m_s$ are the masses for top-partner and $s$ respectively, and $\lambda_i$ are coupling constants. We work in the limit where the coupling $\lambda$ is much larger than $\lambda_{1,2}$ or the electroweak coupling, such that the top-partner decays are predominantly into top and $s$ with almost 100% BR, but is small enough that the width of the top partner remains relatively narrow. In this limit, the relevant parameters are the top partner and scalar masses, with mild dependence on the strength of the interactions. In the more general case where the top partners have appreciable decays into other channels, our results can be rescaled with the corresponding BR and continue to apply.

## 3 Top partner pair production and signatures

For modest mixing, the dominant top partner production mechanism at the LHC is production of a $t'\bar{t}'$ pair through the strong force of which the rate only depends on the partner mass and the strong coupling. The rate at the LHC operating at $\sqrt{s} = 14\,\text{TeV}$ as a function of the top partner mass is shown in the right panel of figure 1.

As with other multi-top final states, it is convenient to classify six top final states based on the decay modes of the $W$ bosons. Leptonic decay modes allow for up to six very energetic charged leptons ($\ell = e, \mu$) in the final state. In table 1, we list the channels containing up to three isolated charged leptons along with their corresponding branching ratios and the primary SM backgrounds leading to topologies similar to a six top final state. Final states with four or more charged leptons are not considered, as the BR for these channels is highly suppressed. While several of these channels have been analyzed at the LHC previously [36–41], which we will discuss later in this section, the focus was on different production mechanism and thus didn't fully capture the feature of six-top final



JHEP10(2019)008

| Channel | Branching Fraction (Truth level) | Event Fraction Reconstructed (1.5 TeV) | SM Backgrounds |
|---|---|---|---|
| 1 Lepton | 17.82% | 38.65% | $t\bar{t}+n$-jets |
| 2 Opposite-Sign Leptons | 8.46% | 9.50% | $t\bar{t}t\bar{t}$ |
| 2 Same-Sign Leptons | 5.36% | 6.51% | $t\bar{t}Z+n$-jets |
| 3 Mixed-Sign Leptons | 5.64% | 3.67% | $t\bar{t}W+n$-jets |
| 3 Same-Sign Leptons | 0.60% | 0.71% | |

**Table 1**. Analysis channels arising from six-top final states with corresponding branch fraction, organized according to the number of leptons in the final state. The events fraction including possible mixing between different channels when considering mis-identification and detector effects for $m_{t'} = 1500\,\text{GeV}$ are listed in the third column. Note that the around 1% lepton fake rate from the jets which results in more leptons due to the large multiplicity of the jets in each events. Dominant SM backgrounds are also listed in the last column.

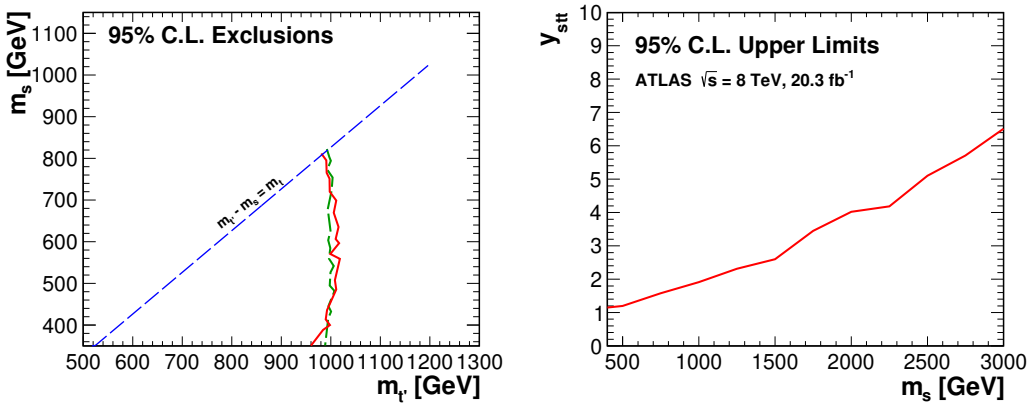


**Figure 2**. Left: current constraints on the $m_s$-$m_{t'}$ plane from the LHC as implemented in CheckMATE. The red line shows the boundary of the excluded region based on the analysis of ref. [36], and the green dashed line corresponds to ref. [37]. Right: upper limit on the $s$-$t$-$\bar{t}$ coupling strength as a function of $m_s$ from LHC searches for top pair production through scalar resonance [42].

states. A six top final state also allows for the new, not previously analyzed, signatures such as three same-sign charged leptons.

In addition to channels with various numbers of leptons, there are several other generic features which commonly appear in the six top signature, including:

- Large $H_T \equiv \sum_i |p_T^i|$ (where the index runs over all visible final state particles), typically $\gtrsim 2000\,\text{GeV}$ for the range of $m_{t'}$ under consideration;
- Boosted top jets which may appear as fat jets in the detector;
- High multiplicity of bottom-flavored and/or light jets.

### 3.1 Current constraints

Most searches for top partners at the LHC have considered missing transverse momentum signatures (based on SUSY searches [43–45]) which occur in theories in which the top



JHEP10(2019)008

partner is connected to a dark matter candidate. These searches exclude scalar top partners with masses up to 900–1000 GeV, depending on the mass of the dark matter candidate. We evaluate the constraints from current searches at the LHC using `CheckMATE` [46] which generates the events corresponding to specific analysis by `MadGraph5` [47] and `PYTHIA8` [48] and performs the analysis according to configuration files.[2] The most stringent constraints are coming from multi-lepton (red line) [36] and multi top quarks searches (green line) [37]. These constraints exclude cross section $\sigma(pp \to t'\bar{t}') < 28.63\,\text{fb}$ at the 95% C.L. for $\sqrt{s} = 13\,\text{TeV}$, corresponding to top partner masses up to nearly 1 TeV.

There is also the possibility to directly produce the $s$ from gluon fusion, which results in a $t\bar{t}$ final state whose invariant mass is resonantly enhanced at $m_s$. In the right panel of figure 2, we show the observational upper limit derived from 8 TeV LHC search for resonant top pair production [42] on the $s$-$t$-$\bar{t}$ coupling strength as a function of the $s$ mass. Note that, here we only present the constraints from 8 TeV analysis. New 13 TeV searches [49] will definitely improve the sensitivity. However, the detailed reanalysis of the 13 TeV result in our scheme is beyond our scope, we leave this for future works.

## 4 Identifying six top events at the LHC

We divide our analysis into channels with 1, 2 or 3 isolated leptons (1, 2, 3-$\ell$) in the final state. The 2- and 3-lepton channels are further divided according to the charges of the isolated leptons. Hence in total, we have five different channels: 1-lepton, 2 opposite sign leptons (2-os$\ell$), 2 same sign leptons (2-ss$\ell$), 3 mixed sign leptons (3-ms$\ell$) and 3 same sign leptons (3-ss$\ell$). These channels are by definition orthogonal to each other, such that a direct combination is straightforward.

### 4.1 Simulation and event reconstruction

We simulate signal and background events for the LHC running at $\sqrt{s} = 14\,\text{TeV}$. Events are generated at the parton level via the `MadGraph5` package [47], using `CTEQ6L` parton distribution functions (PDFs) [50]. Resonances are decayed either via `MadSpin` [51] for top quarks and $W$ bosons, or `PYTHIA8` [48] for the top partners. Parton level events are then passed to `PYTHIA8` for initial state radiation, showering and hadronization. The detector reconstruction is simulated by `Delphes` [52] using the default CMS configuration with modified lepton isolation and b-tagging efficiency (described below). Selection cuts are imposed through the `ROOT` framework via the PyROOT interface, with `FastJet` [53] providing further jet reconstruction and clustering analysis.

The signal process is generated as $pp \to t'\bar{t}'$ for the set of top partner masses $m_{t'} = 1.0$, 1.3, 1.5, 1.8, 2.0 and 2.5 TeV. As mentioned above, `PYTHIA8` decays the top partners into top quarks via $t' \to ts \to t\bar{t}t$, with an assumed 100% branching ratio. This process loses information regarding spin correlations, and thus we do not explore related observables in

[2] 'Analysis' means a set of modified Delphes card, signal regions, cut flows, observed event number according to ATLAS/CMS's paper. What we used are all public on the homepage of the CheckMATE. And then determine whether the parameter point is excluded or not. The results are shown in the $m_{t'}$-$m_s$ plane in the left panel of figure 2.



JHEP10(2019)008

this analysis. For each choice of $m_{t'}$, we fix the singlet mass to be $m_s = m_{t'} - 500$ GeV. While this choice is not general, our analysis does not rely on any selection related to this choice, and so we expect the derived efficiencies to be roughly independent of $m_s$. However, the spectrum will also affect the momentum of $m_t$ and thus affect final results through fat jet reconstruction and top-tagging that we will discuss later. We have checked the effects by varying the mass of $s$ for fixing $m_{t'}$. We find that the event selection efficiency do have some small difference, however, when taking into account the statistic uncertainties, the final sensitivity do not change too much. Hence, for simplicity, we fix the singlet mass to be $m_s = m_{t'} - 500\,\text{GeV}$ throughout the whole analysis.

The background processes are generated as:

- $t\bar{t} + 3j$;
- $t\bar{t} + W/Z + 2j$;
- $t\bar{t}t\bar{t}$.

with a cut of $H_T > 1.5$ TeV imposed at the generator level to improve reconstruction efficiency. Even with this selection, we are computationally limited to processes with at most five final state particles, and restrict ourselves to sufficiently inclusive quantities in our analysis such that this limitation is unlikely to be important. We incorporate the possibility of "lepton charge flip" manually according to the prescription in ref. [54].

After the detector simulation, physics-level objects are reconstructed in both signal and background processes as:

- Leptons are required to be isolated according to the prescription in ref. [55].
- Jets are reconstructed using the anti-$k_T$ algorithm [56] with $r = 0.4$ and $p_T > 30\,\text{GeV}$;
- Fat jets are reconstructed using anti-$k_T$ with $r = 1.0$ and $p_T > 200\,\text{GeV}$;
- Jets are bottom-tagged according to the DeepFlavor performance shown in ref. [57] using the 70% tagging efficiency as the work point;
- Tops are tagged using a convolutional neural network (CNN) described in appendix A at the 50% benchmark operating point.

These reconstructed objects are fed into the selection described below to assess how well the signal may be extracted from the background. The distributions of $H_T$, $n_{fj}$ (number of fat jets), $n_{tfj}$ (number of top-tagged jets) and $n_b$ (number of b-tagged jets) from the SM background and the signal (with two choices of top partner mass, 1.5 TeV (red line) and 2.5 TeV (orange line)) are shown in figure 3 for the 3 mixed sign leptons case. We can clearly see from this figure that $H_T$ of the signal process is usually larger than the background processes and will increase with the mass of the top partner, $m_{t'}$. The same behavior also appears in the distributions of $n_{fj}$ and $n_{tfj}$, as the more boosted jet is easier to be reconstructed as fat jets and further identified as top jets. The last distribution of $n_b$ is almost independent of $m_{t'}$, as it is almost controlled by the true number of the $b$-jets in the events, and we model the $b$-tagging efficiency as a constant (70% as described above) throughout the central region.



JHEP10(2019)008

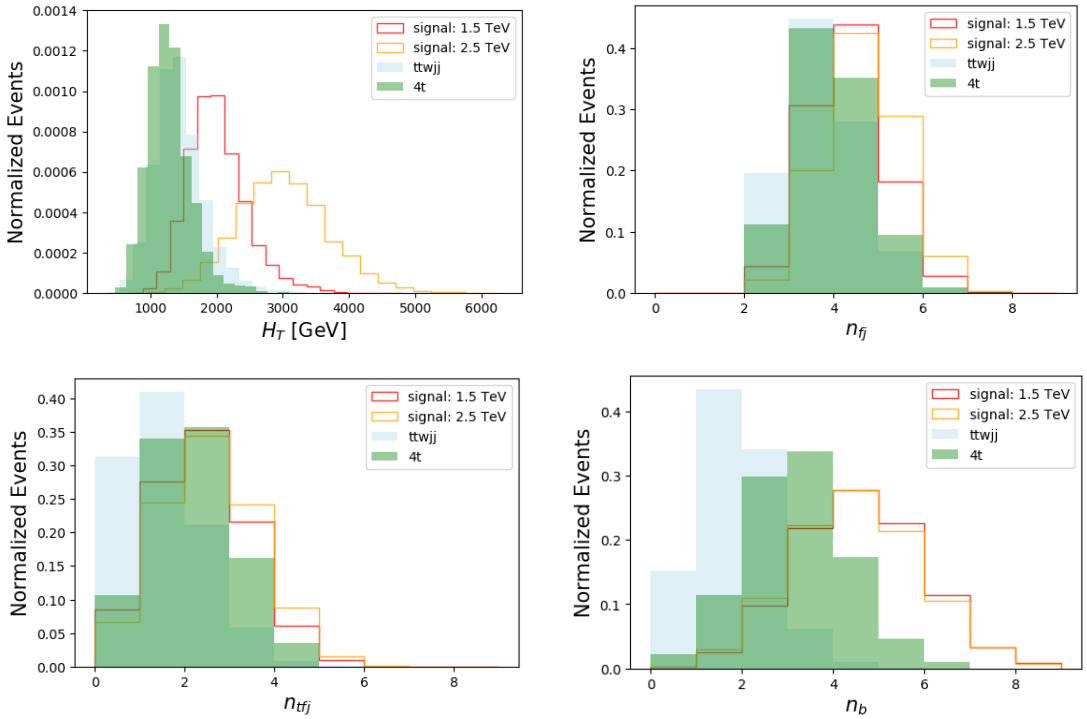


**Figure 3**. The distribution of $H_T$ (top left), $n_{fj}$ (top right), $n_{tfj}$ (bottom left) and $n_b$ (bottom right) of the signal and backgrounds for the 3 mixed sign leptons case. Two choices of the top partner mass, $m_{t'}$, are presented: 1.5 TeV (red line) and 2.5 TeV (orange line).

### 4.2 Event selection and sensitivity

We sort our events into five channels based on the number (and charge) of the leptons they contain as described above. The event fractions for each channel considering the detector effects are also listed in the third column of table 1. Note that we also include 1% lepton fake rate from jets which results in more leptons than expected just from the branch fraction due to the large multiplicity of jets in the events. For channels with two or more leptons, we eliminate $\mid m_{\ell\ell} - m_Z \mid < 5$ GeV to reduce background from the $Z$ pole. At this Pre-Cut selection level, we also require $H_T \geq 2000$ GeV.

After the Pre-Cuts, for $m_{t'} = 1.5\,\text{TeV}$, the signal of 1-$\ell$ and 2-$\ell$ channel is typically 10–100 times smaller than the sum of the backgrounds, while other channels have similar with or even larger signal than the backgrounds. We further optimize the significance of the top partner signal by considering following kinematic variables (Cut I):

- The number of fat jets $n_{fj} \geq 3$;
- The number of top tagged fat jets $n_{tfj} \geq 1$;
- The number of $b$-tagged jets $n_b \geq 5$.

The number of normal jets $n_j$ seems to be another useful discriminant. However, we find that the number of normal jets outside the fat-jet cone is almost the same between



JHEP10(2019)008

| Channels | Process | Pre Cut [fb] | Cut I [fb] | Significance [3ab$^{-1}$] |
|---|---|---|---|---|
| 1-$\ell$ | signal | $6.60 \times 10^{-1}$ | $2.80 \times 10^{-1}$ | 20.47 |
| | $t_\ell t_q jjj$ | $8.28 \times 10^{1}$ | $4.72 \times 10^{-1}$ | |
| | $t\bar{t}t\bar{t}$ | $3.97 \times 10^{-2}$ | $3.27 \times 10^{-3}$ | |
| 2-os$\ell$ | signal | $1.40 \times 10^{-1}$ | $5.36 \times 10^{-2}$ | 17.99 |
| | $t_\ell t_\ell jjj$ | $4.71 \times 10^{0}$ | $1.32 \times 10^{-2}$ | |
| | $t_\ell t_q W_\ell jj$ | $3.01 \times 10^{-1}$ | $7.70 \times 10^{-5}$ | |
| | $t\bar{t}t\bar{t}$ | $4.14 \times 10^{-3}$ | $2.54 \times 10^{-4}$ | |
| 3-ms$\ell$ | signal | $4.30 \times 10^{-2}$ | $1.45 \times 10^{-2}$ | 21.41 |
| | $t_\ell t_\ell W_\ell jj$ | $5.30 \times 10^{-3}$ | $5.89 \times 10^{-6}$ | |
| | $t\bar{t}t\bar{t}$ | $4.36 \times 10^{-4}$ | $2.25 \times 10^{-5}$ | |
| 2-ss$\ell$ | signal | $9.57 \times 10^{-2}$ | $3.67 \times 10^{-2}$ | 30.65 |
| | $t_\ell t_q W_\ell jj$ | $2.91 \times 10^{-2}$ | $6.48 \times 10^{-5}$ | |
| | $t\bar{t}t\bar{t}$ | $2.11 \times 10^{-3}$ | $1.31 \times 10^{-4}$ | |
| 3-ss$\ell$ | signal | $7.16 \times 10^{-3}$ | / | 11.48 |
| | $t_\ell t_q W_\ell jj$ | $6.45 \times 10^{-5}$ | / | |
| | $t_\ell t_q Z_{\ell\ell}$ | $7.05 \times 10^{-5}$ | / | |
| Total Significance: | | | | 47.69 |

**Table 2**. Cut flow for $m_{t'} = 1.5$ TeV of all five channels with different number of leptons. The corresponding significance with 3 ab$^{-1}$ luminosity for different channels and the combined significance are also list in the last column. Note that for 3-ss$\ell$ channel, we do not apply Cut I, as the event rate is already extremely low, further selection will decrease the sensitivity.

signal and background. The difference mainly comes from normal jets inside the fat-jet cone, which we've already considered when tagging the top fat jet. Hence, we do not use $n_j$ further.

For each channel, the cross section of the signal (for $m_{t'} = 1.5$ TeV) and corresponding backgrounds after each set of cuts, and the statistical significance of that channel (assuming 3 ab$^{-1}$ of integrated luminosity) are summarized in table 2. We find that the single best channel is the one demanding two same sign charged leptons, which balances rate against standing out from the background.

For each value of $m_{t'}$, we repeat this procedure for the same set of cuts. In each case, assuming that the top partners are pair produced exclusively through the strong force, the sensitivity maps into a bound on the branching ratio for $t' \to ts \to t\bar{t}t$. In figure 4, we show the limit on this branching ratio as a function of $m_{t'}$ from 1000 GeV to 2500 GeV. As $m_{t'}$ approaches 2500 GeV, the upper limit on the branching ratio approaches 1, implying that higher masses will only be accessible if there is an additional mechanism responsible for producing $t'\bar{t}'$ beyond the strong interaction.

### 4.3 Reconstructing $m_{t'}$

In the case that an excess is detected, it would be desirable to reconstruct the origin of the signal from top partner pair production, and determine the $t'$ mass. Direct reconstruction



JHEP10(2019)008

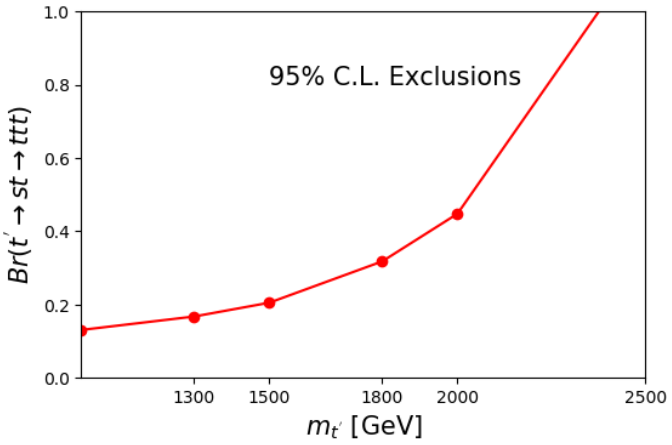


**Figure 4**. The 95% C.L. upper limit with $L = 3000\,\text{fb}^{-1}$ on the branch fraction of $t' \to st \to t\bar{t}t$ as a function of top-partner mass $m_{t'}$.

as an invariant mass is challenging, since the leptonic top decays produce undetectable neutrino which results in missing momentum, and the decay products of six top quarks result in a large combinatoric confusion.

In order to improve the sensitivity to the mass, another CNN is trained to predict the probability that a set of events originate from a particular value of $m_{t'}$. This CNN has similar structure as the one explained in appendix A (the differences are also explained there). However, instead of the data associated with one particular jet, the whole $p_T$ distribution in the calorimeter for the event after converting into "tensor image" is used as the input of the CNN. Using the whole $p_T$ distribution in one event actually captures following two features:[3]

- The $H_T$ distribution, the sum of the $p_T$ of all visible particles, which increases with $m_{t'}$;
- The dispersion, which describes the $p_T$ distribution in the whole space, which decreases with $m_{t'}$.

We show the output distribution for the 1.5 TeV classifier when fed simulated events with a variety of values of $m_{t'}$ in the left panel of figure 5. For simplicity, we neglect the background in this assessment; while this is not a good approximation for all of the channels, it well approximates the channels with the largest sensitivity (such as 2-ss$\ell$). We leave a more realistic analysis for future work.

Based on the distributions shown in the left panel of figure 5, a binned likelihood is constructed and its negative log-likelihood is shown in the middle panel of figure 5. Also for comparison, the result corresponding to the $H_T$ distribution alone is also presented, illustrating the increase in sensitivity achieved by the CNN. A more detailed analysis for 1.5 TeV case is shown in the right panel of figure 5, and an $\mathcal{O}(100)$ GeV determination of the top partner mass can be achieved.

[3]Note that, in principle, we can also use Boost Decision Tree (BDT) for this task, however, the second



JHEP10(2019)008

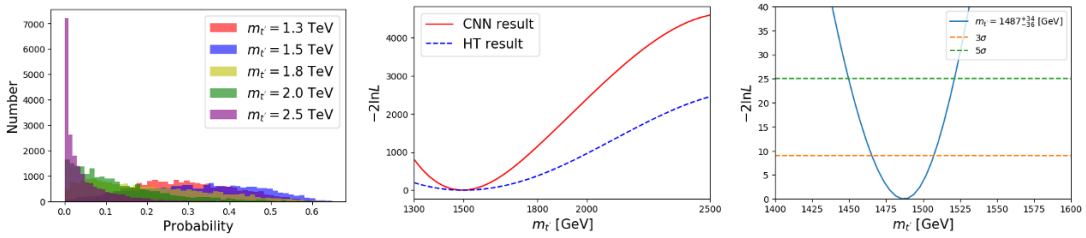


**Figure 5**. Left panel: the CNN output for the 1.5 TeV classifier when fed events corresponding to different values of $m_{t'}$ as indicated. Middle panel: the $-2\ln L$ constructed from the distribution from CNN output (red) and the $H_T$ distribution(blue) aimed for $m_{t'} = 1.5$ TeV as a function of the hypothesized mass. Right panel: the $-2\ln L$ analysis around $m_{t'} \sim 1.5$ TeV.

## 5 Conclusions

Events containing six top quarks are within grasp of the LHC Run 3, and provide a fascinating laboratory to search for physics beyond the Standard Model. We have explored a simplified model which arises as the low energy limit of compelling theories of a composite Higgs, and in which top partners decay into three top quarks with a large branching ratio. We have constructed inclusive observables which are able to tease the signal out of the otherwise large Standard Model background, and find that top partner masses up to around 2.5 TeV are accessible with $\sim 3$ ab$^{-1}$ as can be seen from figure 4.

Further, the distribution of the final state particles also provides information about the mass of the top partner. A CNN-based method is used to investigate how well one can determine the top partner mass, with the whole $p_T$ distribution over the calorimeter used as the input to the CNN. As shown in figure 5, around 1.5 TeV, an $\mathcal{O}(100)$ GeV determination of the mass can be achieved.

## Acknowledgments

Y.W. is supported by the Natural Sciences and Engineering Research Council of Canada (NSERC). T.M.P.T. is supported in part by the US National Science Foundation through NSF Grant No. PHY-1620638. J.S. is supported by the National Natural Science Foundation of China (NSFC) under grant No.11647601, No.11690022, No.11851302, No.11675243 and No.11761141011 and also supported by the Strategic Priority Research Program of the Chinese Academy of Sciences under grant No.XDB21010200 and No.XDB23000000. H.H. is supported in part by NSFC under grant No.11847151 and the Education Department of Guizhou Province under grant No.KY[2017]004, and also supported by the 2018 scientific research startup foundation for the introduced talent of Guizhou University of Finance and Economics under grant No.2018YJ61. T.M. is supported in part by project Y6Y2581B11 supported by 2016 National Postdoctoral Program for Innovative Talents. The simulations for this work were done in part at the HPC Cluster of ITP-CAS.

feature is not explicitly expressed in terms of several physical variables. Thus, a similar CNN as the one we used for top-tagging is used here for our own convenience.



JHEP10(2019)008

(a) CNN for top tagging

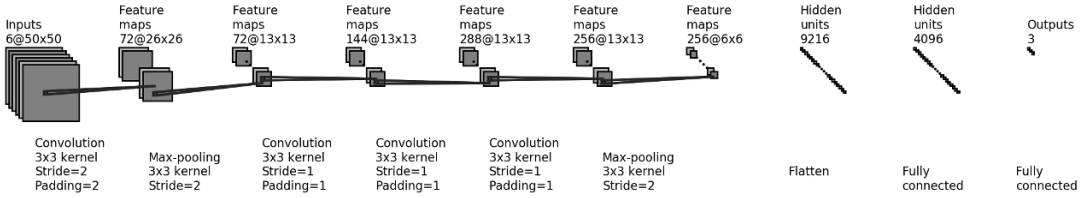


(b) CNN for top partner mass construction

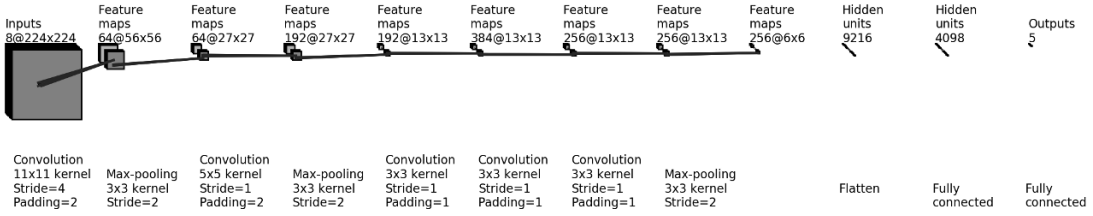


**Figure 6**. The structure of the CNN used for top tagging (upper panel) and top partner mass construction (lower panel).

## A Boosted jet tagging

Our jet classification is based on a Convolutional Neutral Network (CNN) which combines calorimeter and tracker information for each fat jet to assign the probabilities that the jet originates from a top, $W$ boson or light parton. For recent work on related strategies, see refs. [6, 58–62].

The training and testing samples are generated through the same procedure as for the signal and background events, simulating the processes $pp \to XX$ with $X = j$, $t$ and $W$. After reconstructing the fat jets using the anti-$k_t$ algorithm with $\Delta R = 1.0$ and $p_T > 200$ GeV, each of them is converted into a "tensor image". A square region in the $(\eta, \phi)$ plane of size $1.0 \times 1.0$ is constructed centered at the center of the jet and divided into $50 \times 50$ equal-sized pixels. Each pixel records the total incident $p_T$ and the multiplicities of both the track and tower classes (from `Delphes`). This results in a six-channel image with dimensions $50 \times 50 \times 6$, which are $p_T$ of tower, $p_T$ of track, $p_T$ of all, multiplicity of tower, multiplicity of track and multiplicity of all.

The tensor image serves as the input to the CNN constructed using the `PyTorch` framework. The CNN consists of the following elements:

- Four convolutional layers with a Rectified Linear Unit (ReLU) activation function;
- Two *max-pooling* layers;
- Classification block layers, including two linear layers with a dropout of 50% probability and ReLU activation function;
- Final linear layer classifying the jet images into different categories.

The detailed structure (including the kernel size, stride size, padding size etc.) of this CNN is shown in the upper panel of figure 6. We also need to notice that for the top partner mass



JHEP10(2019)008

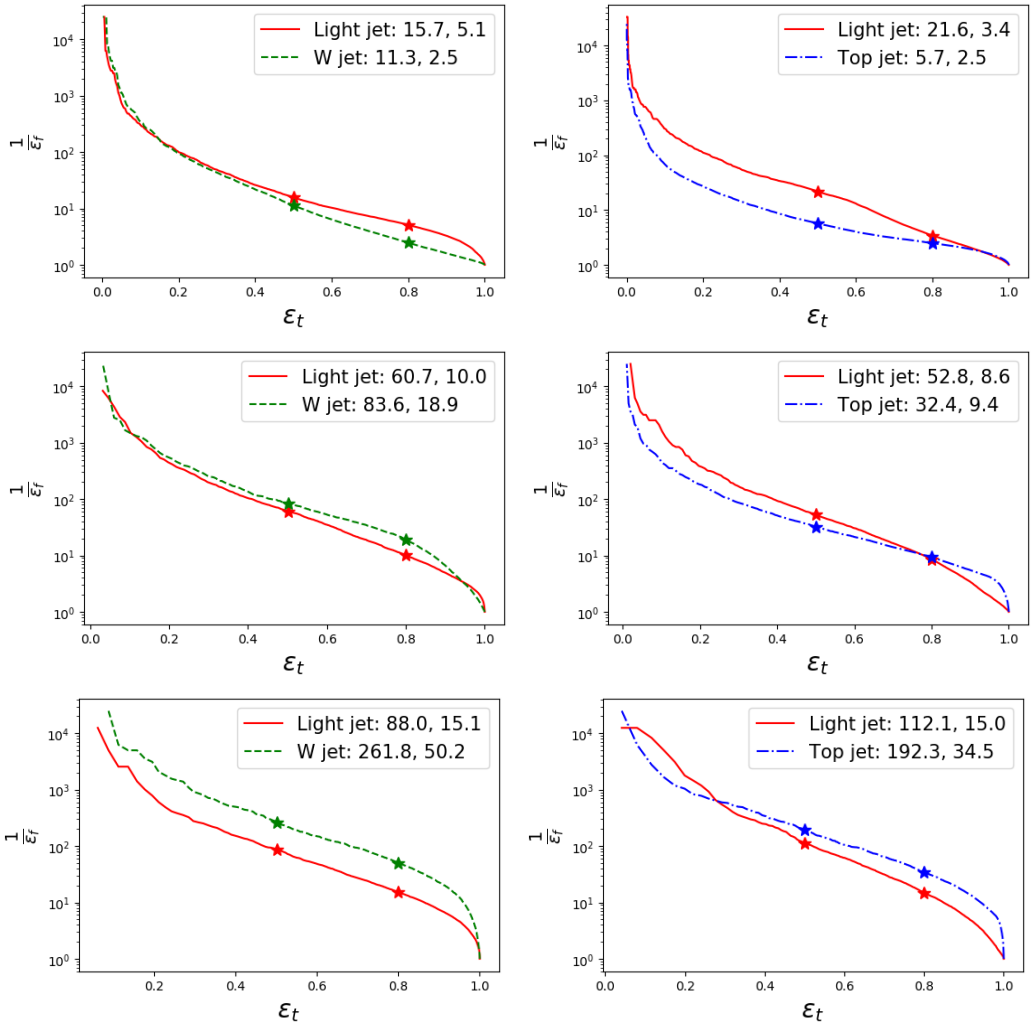


**Figure 7**. The ROC curves for tagging a top (left column) against a light jet (red straight) or $W$ (green dash); or for tagging a $W$ boson (right column) against a light jet (red straight) or top (blue dash point), for $p_T$ ranges are [200, 400] GeV, [400, 800] GeV and $>$ 800 GeV for the upper, middle and lower rows. The x axis is $\epsilon_t$ and y axis is $\frac{1}{\epsilon_f}$, which $\epsilon_t$ is the "true rate" and $\epsilon_f$ is the "mistagging rate". Benchmark points with top tagging rates of 0.5 and 0.8 are indicated on each curve, with the corresponding $\epsilon_f$.

input, we considered the $p_T$ and multiplicity for the `EFlowPhoton`, `EFlowNeutralHadron` and `EFlowTracks` in `Delphes` so that the input is 8.

In each sample, jets are divided into three bins according to their $p_T$: 200 GeV $< p_T^{\text{jet}} <$ 400 GeV, 400 GeV $< p_T^{\text{jet}} <$ 800 GeV and $p_T^{\text{jet}} >$ 800 GeV, and the CNN is trained separately for each $p_T$ bin. The tagging performance is characterized by the *Receiver Operating Characteristic* (ROC) curve. For each pair of jet classes $j_1$ and $j_2$ (tagging $j_1$ against $j_2$), the ROC curve (see figure 7) shows the "tagging efficiency" (the probability of correctly tagging the jet of class $j_1$ as $j_1$) on the horizontal axis, and 1-"mistagging rate" (the probability of incorrectly tagging jet of class $j_2$ as $j_1$) on the vertical axis.



JHEP10(2019)008

In figure 7, the left panels show the ROC curves for tagging a top quark against a $W$-boson and a light jet, while the right panels are the ROC curves for tagging a $W$ boson against a top quark and a light jet. The top, middle and bottom panels correspond to the $p_T$ bins: [200,400] GeV, [400,800] GeV and [800,$\infty$] GeV, respectively. As expected, higher $p_T$ tops and $W$s are identified much more efficiently. Two benchmark working points corresponding to 50% and 80% efficiency for top tagging are marked on each curve in figure 7, and the corresponding mistagging rates are listed in the legend of each panel. In practice, the 50% working point is used to tag the top jets.



JHEP10(2019)008

## References

[1] J.L. Feng, *Naturalness and the status of supersymmetry*, *Ann. Rev. Nucl. Part. Sci.* **63** (2013) 351 [arXiv:1302.6587] [INSPIRE].

[2] G.F. Giudice, *Naturalness after LHC8*, PoS(EPS-HEP 2013)163 [arXiv:1307.7879] [INSPIRE].

[3] G. Altarelli, *The Higgs: so simple yet so unnatural*, *Phys. Scripta* **T 158** (2013) 014011 [arXiv:1308.0545] [INSPIRE].

[4] M. Farina, D. Pappadopulo and A. Strumia, *A modified naturalness principle and its experimental tests*, *JHEP* **08** (2013) 022 [arXiv:1303.7244] [INSPIRE].

[5] A. de Gouvêa, D. Hernandez and T.M.P. Tait, *Criteria for natural hierarchies*, *Phys. Rev.* **D 89** (2014) 115005 [arXiv:1402.2658] [INSPIRE].

[6] C. Csáki et al., *Naturalness sum rules and their collider tests*, *JHEP* **05** (2019) 132 [arXiv:1811.01961] [INSPIRE].

[7] C.-R. Chen et al., *Testing naturalness at* 100 *TeV*, *JHEP* **09** (2017) 129 [arXiv:1705.07743] [INSPIRE].

[8] R. Contino and G. Servant, *Discovering the top partners at the LHC using same-sign dilepton final states*, *JHEP* **06** (2008) 026 [arXiv:0801.1679] [INSPIRE].

[9] A. Atre et al., *Model-independent searches for new quarks at the LHC*, *JHEP* **08** (2011) 080 [arXiv:1102.1987] [INSPIRE].

[10] G. Cacciapaglia et al., *Heavy vector-like top partners at the LHC and flavour constraints*, *JHEP* **03** (2012) 070 [arXiv:1108.6329] [INSPIRE].

[11] A. De Simone, O. Matsedonskyi, R. Rattazzi and A. Wulzer, *A first top partner hunter's guide*, *JHEP* **04** (2013) 004 [arXiv:1211.5663] [INSPIRE].

[12] J. Mrazek and A. Wulzer, *A strong sector at the LHC: top partners in same-sign dileptons*, *Phys. Rev.* **D 81** (2010) 075006 [arXiv:0909.3977] [INSPIRE].

[13] A. Azatov, M. Salvarezza, M. Son and M. Spannowsky, *Boosting top partner searches in composite Higgs models*, *Phys. Rev.* **D 89** (2014) 075001 [arXiv:1308.6601] [INSPIRE].

[14] M. Backović, T. Flacke, S.J. Lee and G. Perez, *LHC top partner searches beyond the 2 TeV mass region*, *JHEP* **09** (2015) 022 [arXiv:1409.0409] [INSPIRE].

[15] O. Matsedonskyi, G. Panico and A. Wulzer, *On the interpretation of top partners searches*, *JHEP* **12** (2014) 097 [arXiv:1409.0100] [INSPIRE].

[16] N. Bizot, G. Cacciapaglia and T. Flacke, *Common exotic decays of top partners*, *JHEP* **06** (2018) 065 [arXiv:1803.00021] [INSPIRE].

[17] S.-S. Xue, *An effective strong-coupling theory of composite particles in UV-domain*, *JHEP* **05** (2017) 146 [arXiv:1601.06845] [INSPIRE].

[18] K.-P. Xie, G. Cacciapaglia and T. Flacke, *Exotic decays of top partners with charge* 5/3*: bounds and opportunities*, arXiv:1907.05894 [INSPIRE].

[19] B. Lillie, J. Shu and T.M.P. Tait, *Top compositeness at the Tevatron and LHC*, *JHEP* **04** (2008) 087 [arXiv:0712.3057] [INSPIRE].

[20] A. Pomarol and J. Serra, *Top quark compositeness: feasibility and implications*, *Phys. Rev.* **D 78** (2008) 074026 [arXiv:0806.3247] [INSPIRE].

[21] C.-R. Chen, W. Klemm, V. Rentala and K. Wang, *Color sextet scalars at the CERN Large Hadron Collider*, *Phys. Rev.* **D 79** (2009) 054002 [arXiv:0811.2105] [INSPIRE].

[22] K. Kumar, T.M.P. Tait and R. Vega-Morales, *Manifestations of top compositeness at colliders*, *JHEP* **05** (2009) 022 [arXiv:0901.3808] [INSPIRE].

[23] T. Gregoire, E. Katz and V. Sanz, *Four top quarks in extensions of the standard model*, *Phys. Rev.* **D 85** (2012) 055024 [arXiv:1101.1294] [INSPIRE].

[24] A. Deandrea and N. Deutschmann, *Multi-tops at the LHC*, *JHEP* **08** (2014) 134 [arXiv:1405.6119] [INSPIRE].

[25] CMS collaboration, *Search for standard model production of four top quarks with same-sign and multilepton final states in proton-proton collisions at* $\sqrt{s} = 13$ *TeV*, *Eur. Phys. J.* **C 78** (2018) 140 [arXiv:1710.10614] [INSPIRE].

[26] ATLAS collaboration, *Search for four-top-quark production in the single-lepton and opposite-sign dilepton final states in pp collisions at* $\sqrt{s} = 13$ *TeV with the ATLAS detector*, *Phys. Rev.* **D 99** (2019) 052009 [arXiv:1811.02305] [INSPIRE].

[27] C. Csáki, T. Ma and J. Shu, *Trigonometric parity for composite Higgs models*, *Phys. Rev. Lett.* **121** (2018) 231801 [arXiv:1709.08636] [INSPIRE].

[28] T.A. Ryttov and F. Sannino, *Ultra minimal technicolor and its dark matter TIMP*, *Phys. Rev.* **D 78** (2008) 115010 [arXiv:0809.0713] [INSPIRE].

[29] J. Galloway, J.A. Evans, M.A. Luty and R.A. Tacchi, *Minimal conformal technicolor and precision electroweak tests*, *JHEP* **10** (2010) 086 [arXiv:1001.1361] [INSPIRE].

[30] B. Gripaios, A. Pomarol, F. Riva and J. Serra, *Beyond the minimal composite Higgs model*, *JHEP* **04** (2009) 070 [arXiv:0902.1483] [INSPIRE].

[31] M. Frigerio, A. Pomarol, F. Riva and A. Urbano, *Composite scalar dark matter*, *JHEP* **07** (2012) 015 [arXiv:1204.2808] [INSPIRE].

[32] J. Serra and R. Torre, *Neutral naturalness from the brother-Higgs model*, *Phys. Rev.* **D 97** (2018) 035017 [arXiv:1709.05399] [INSPIRE].

[33] T. Ma and G. Cacciapaglia, *Fundamental composite 2HDM:* SU($N$) *with* 4 *flavours*, *JHEP* **03** (2016) 211 [arXiv:1508.07014] [INSPIRE].

[34] Y. Wu, T. Ma, B. Zhang and G. Cacciapaglia, *Composite dark matter and Higgs*, *JHEP* **11** (2017) 058 [arXiv:1703.06903] [INSPIRE].

[35] G. Cacciapaglia, S. Vatani, T. Ma and Y. Wu, *Towards a fundamental safe theory of composite Higgs and Dark Matter*, arXiv:1812.04005 [INSPIRE].

JHEP10(2019)008

[36] ATLAS collaboration, *Search for supersymmetry at $\sqrt{s} = 13$ TeV in final states with jets and two same-sign leptons or three leptons with the ATLAS detector*, *Eur. Phys. J.* **C 76** (2016) 259 [arXiv:1602.09058] [INSPIRE].

[37] ATLAS collaboration, *Search for production of vector-like top quark pairs and of four top quarks in the lepton-plus-jets final state in pp collisions at $\sqrt{s} = 13$ TeV with the ATLAS detector*, ATLAS-CONF-2016-013 (2016).

[38] ATLAS collaboration, *Search for supersymmetry in final states with two same-sign or three leptons and jets using 36 $fb^{-1}$ of $\sqrt{s} = 13$ TeV pp collision data with the ATLAS detector*, *JHEP* **09** (2017) 084 [*Erratum ibid.* **08** (2019) 121] [arXiv:1706.03731] [INSPIRE].

[39] ATLAS collaboration, *Search for supersymmetry in events with four or more leptons in $\sqrt{s} = 13$ TeV pp collisions with ATLAS*, *Phys. Rev.* **D 98** (2018) 032009 [arXiv:1804.03602] [INSPIRE].

[40] CMS collaboration, *Search for electroweak production of charginos and neutralinos in multilepton final states in proton-proton collisions at $\sqrt{s} = 13$ TeV*, *JHEP* **03** (2018) 166 [arXiv:1709.05406] [INSPIRE].

[41] CMS collaboration, *Search for new phenomena with multiple charged leptons in proton-proton collisions at $\sqrt{s} = 13$ TeV*, *Eur. Phys. J.* **C 77** (2017) 635 [arXiv:1701.06940] [INSPIRE].

[42] ATLAS collaboration, *A search for $t\bar{t}$ resonances using lepton-plus-jets events in proton-proton collisions at $\sqrt{s} = 8$ TeV with the ATLAS detector*, *JHEP* **08** (2015) 148 [arXiv:1505.07018] [INSPIRE].

[43] ATLAS collaboration, *Search for direct top squark pair production in final states with two leptons in $\sqrt{s} = 13$ TeV pp collisions with the ATLAS detector*, *Eur. Phys. J.* **C 77** (2017) 898 [arXiv:1708.03247] [INSPIRE].

[44] ATLAS collaboration, *Search for a scalar partner of the top quark in the jets plus missing transverse momentum final state at $\sqrt{s} = 13$ TeV with the ATLAS detector*, *JHEP* **12** (2017) 085 [arXiv:1709.04183] [INSPIRE].

[45] ATLAS collaboration, *Search for top-squark pair production in final states with one lepton, jets and missing transverse momentum using 36 $fb^{-1}$ of $\sqrt{s} = 13$ TeV pp collision data with the ATLAS detector*, *JHEP* **06** (2018) 108 [arXiv:1711.11520] [INSPIRE].

[46] M. Drees et al., *CheckMATE: confronting your favourite new physics model with LHC data*, *Comput. Phys. Commun.* **187** (2015) 227 [arXiv:1312.2591] [INSPIRE].

[47] J. Alwall et al., *The automated computation of tree-level and next-to-leading order differential cross sections and their matching to parton shower simulations*, *JHEP* **07** (2014) 079 [arXiv:1405.0301] [INSPIRE].

[48] T. Sjöstrand et al., *An introduction to PYTHIA 8.2*, *Comput. Phys. Commun.* **191** (2015) 159 [arXiv:1410.3012] [INSPIRE].

[49] ATLAS collaboration, *Search for heavy particles decaying into top-quark pairs using lepton-plus-jets events in proton-proton collisions at $\sqrt{s} = 13$ TeV with the ATLAS detector*, *Eur. Phys. J.* **C 78** (2018) 565 [arXiv:1804.10823] [INSPIRE].

[50] P.M. Nadolsky et al., *Implications of CTEQ global analysis for collider observables*, *Phys. Rev.* **D 78** (2008) 013004 [arXiv:0802.0007] [INSPIRE].

[51] P. Artoisenet, R. Frederix, O. Mattelaer and R. Rietkerk, *Automatic spin-entangled decays of heavy resonances in Monte Carlo simulations*, *JHEP* **03** (2013) 015 [arXiv:1212.3460] [INSPIRE].



JHEP10(2019)008

[52] DELPHES 3 collaboration, *DELPHES 3, a modular framework for fast simulation of a generic collider experiment*, *JHEP* **02** (2014) 057 [arXiv:1307.6346] [INSPIRE].

[53] M. Cacciari, G.P. Salam and G. Soyez, *FastJet user manual*, *Eur. Phys. J.* **C 72** (2012) 1896 [arXiv:1111.6097] [INSPIRE].

[54] ATLAS collaboration, *Search for doubly charged Higgs boson production in multi-lepton final states with the ATLAS detector using proton-proton collisions at* $\sqrt{s} = 13$ *TeV*, *Eur. Phys. J.* **C 78** (2018) 199 [arXiv:1710.09748] [INSPIRE].

[55] CMS collaboration, *Measurements of the* $t\bar{t}$ *production cross section in lepton+jets final states in pp collisions at* 8 *TeV and ratio of* 8 *to* 7 *TeV cross sections*, *Eur. Phys. J.* **C 77** (2017) 15 [arXiv:1602.09024] [INSPIRE].

[56] M. Cacciari, G.P. Salam and G. Soyez, *The anti-*$k_t$ *jet clustering algorithm*, *JHEP* **04** (2008) 063 [arXiv:0802.1189] [INSPIRE].

[57] CMS collaboration, *CMS Phase 1 heavy flavour identification performance and developments*, CMS-DP-2017-013 (2017).

[58] T. Plehn and M. Spannowsky, *Top tagging*, *J. Phys.* **G 39** (2012) 083001 [arXiv:1112.4441] [INSPIRE].

[59] G. Kasieczka, T. Plehn, M. Russell and T. Schell, *Deep-learning top taggers or the end of QCD?*, *JHEP* **05** (2017) 006 [arXiv:1701.08784] [INSPIRE].

[60] A. Butter, G. Kasieczka, T. Plehn and M. Russell, *Deep-learned top tagging with a Lorentz layer*, *SciPost Phys.* **5** (2018) 028 [arXiv:1707.08966] [INSPIRE].

[61] M. Dasgupta, M. Guzzi, J. Rawling and G. Soyez, *Top tagging: an analytical perspective*, *JHEP* **09** (2018) 170 [arXiv:1807.04767] [INSPIRE].

[62] S. Macaluso and D. Shih, *Pulling out all the tops with computer vision and deep learning*, *JHEP* **10** (2018) 121 [arXiv:1803.00107] [INSPIRE].

JHEP10(2019)008